PFC2D Smooth joint contact model numerical experiments

Nathan Deisman
Department of Civil and Environmental Engineering – University of Alberta, Edmonton, Alberta, Canada
Diego Mas Ivars & Matthew Pierce
Itasca Geomekanik AB, Solna, Sweden
Itasca Consulting Group, Inc. Minneapolis, MN, USA

ABSTRACT
The Synthetic Rock Mass (SRM) approach combines the Bonded Particle Model for rock with a Discrete Fracture Network and a Smooth Joint model to numerically examine the behaviour of rock masses. The SRM has been shown to predict the behaviour of a rock mass, however the Smooth Joint model has not been rigorously tested against simple laboratory observations. In this work, numerical experiments have been carried out to determine if the PFC2D Smooth Joint model adequately simulates the observed behaviours of one, two and three flaws embedded in a rock-like material under uniaxial compression. Numerical experiments were also completed to examine the influence of loading rate and sample resolution on the fracturing behaviour.

RÉSUMÉ
La stratégie Synthetic Rock Mass (SRM) est un combinaison du Bonded Particle Model avec Discrete Fracture Network en utilisant le Smooth Joint Model pour analyser numeriquement le comportement des masses rocheuses. SRM prevoit le comportement des masses rocheuses, mais le Smooth Joint Model n'était pas examiné rigoureusement contre les observations laboratoires. Ici, on a fait de l'expériences numériques pour déterminer si le PFC2D Smooth Joint Model suffit en simulation de comportement d'une, deux, et trois défauts dans un substance rocheuse sous pression uniaxial. Les expériences numeriques étaient aussi completées pour examiner l'effets aux taux de chargements, et resolution du prélèvement au comportement de failles.

1 INTRODUCTION

The development of numerical models based on particle mechanics and the advances in computing power now allows for detailed examination of the interaction between rock discontinuities and intact rock at a variety of scales. It is now possible to simulate a rock mass and conduct 'numerical experiments,' analogous in some respects to physical experiments, and to obtain considerable insight into the nature of both size and time effects on the strength and constitutive behavior of rock masses (Fairhurst et al., 2007).

1.1 Synthetic Rock Mass

The Synthetic Rock Mass (SRM) approach is a new methodology for the characterization of the mechanical behaviour of jointed rock masses. The SRM concept allows for rock volumes at multiple scales containing thousands of impersistent pre-existing joints to be subjected to any non-trivial stress path while extracting and/or monitoring a voluminous amount of information regarding the rock mass behaviour. Rock mass properties including anisotropic strength and the full deformation tensor can be extracted from the numerical testing. Other information which can be obtained from the SRM includes brittleness, fragmentation, seismicity, and fracture aperture change (Mas Ivars et al., 2007).

The SRM combines two established concepts, the Bonded Particle Model for rock (BPM) and Discrete Fracture Network (DFN) by inserting several joints through a new Smooth Joint (SJ) particle contact model. The SRM has been shown to represent the behaviour of large rock mass well, however the SJ model has not been rigorously tested against simple laboratory observations.

1.2 Objective of Investigation

The present study was undertaken to assess the ability of the current SJ formulation in PFC2D to simulate crack initiation, propagation and coalescence. Results from several laboratory uniaxial compression tests on one, two and three small flaws embedded in rock-like material are simulated. Strain rate and particle resolution were also tested to investigate their influence on the fracturing behaviour.

2 SMOOTH JOINT MODEL

To date, joints have been modelled in PFC by identifying a joint plane and changing the properties of contacts between particles lying on either side of that plane. This technique created a joint plane with an unrealistically high joint friction angle due to the '*bumpiness*' of the joint. The SJ contact model was developed by Peter Cundall (Pierce et al., 2005) to remedy this shortcoming.

2.1 SJ Contact Model

The SRM is constructed in two phases by first creating a BPM and then inserting the SJ model and assigning joint properties. While the BPM simulates the behaviour of a particle interface normal to the particle contact, n_c (Figure 1), the SJ model allows for an interface in any desired orientation regardless of the local particle contact orientations. This allows two contact particles to displace relative to one another without having to honor local contact orientations, thereby eliminating the need for particles to "ride over" each other to accommodate relative shear displacement.

An SJ contact is shown in Figure 1 with the joint geometry consisting of surfaces 1 and 2 and a dip angle, θ_p. The joint plane orientation is defined by the unit-normal vector, n_j, and perpendicular vector, t_j. When the SJ model is assigned to the contact, ball1 and ball2 are associated with the appropriate joint surfaces. Normal and shear force and displacement are calculated relative to the SJ contact using Coulomb sliding with dilation and then mapped back to the ball1 ball2 contact to update the model (Itasca Consulting Group Inc., 2008).

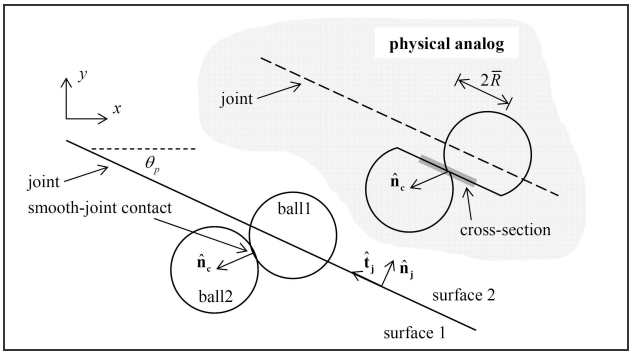

Figure 1. Smooth Joint contact model between ball1 and ball2. Surface 1 and surface 2 denote either side of the joint lying at a dip angle of θ_p (adapted from Itasca Consulting Group Inc., 2008).

2.2 SJ Properties

The SJ model is defined in terms of conventional rock mechanics joint properties obtained from laboratory or field testing. Each joint can be assigned a friction coefficient (or angle), cohesion, tension and shear and normal stiffness. The shear and normal force acting on the joint can be tracked during simulation, as well as the normal and shear displacement.

3 NUMERICAL SIMULATIONS

A series of experimental results on simulated rock material containing one, two, and three flaws orientated with different flaw angles, bridge angles and bridge distances were selected from the literature for numerical simulation. The selection criteria included documentation on intact strength, deformation properties, specimen and flaw geometries, photographs of fracturing, and other parameters such as crack initiation angles and locations. The selected laboratory results were further divided into two sub groups containing strong material (one flaw) and a weak material (two and three flaws) which enabled SJ testing in two significantly different materials.

In each case the intact material was matched using a resolution of eight particles across the diameter of a single SJ, and then the SJ was inserted with reported properties. The results were qualitatively and quantitatively compared to reported fracture coalescence patterns and strength results.

3.1 Resolution

The number and size distribution of particles defining a BPM influence the macro properties of the model, which is why each BPM requires micro property calibration. Typically an SRM simulation employs a particle resolution across the diameter of an SJ somewhere between five and ten. The minimum particle radius (R_{min}) and maximum to minimum particle size ratio (R_{max}/R_{min}) can be used to calculate the resolution (Res) of a dimension (L) through Eq 1.

$$Res = (L/R_{min})[1/(1+R_{max}/R_{min})] \quad [1]$$

3.2 One Flaw

Wong and Einstein (2006) presented experimental results on single flaws with a length of 12.7 mm at multiple angles embedded in a laboratory created gypsum specimen (Figure 2). The intact material had dimensions h:w:t of 156:76:32 mm with a UCS of 34.5 MPa, Brazilian tensile strength of 3.2 MPa, E of 5960 MPa and Poisson's ratio of 0.15. The study measured the distances and angles at which fractures began to appear relative to the initial flaw tip as well as tensile wing crack initiation stress.

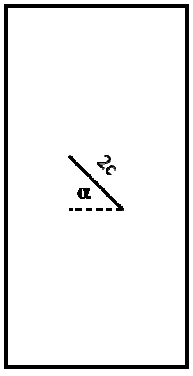

Test ID	α (°)
1-1	0
1-2	15
1-3	30
1-4	35
1-5	40
1-6	45
1-7	50
1-8	55
1-9	60
1-10	70
1-11	75

Figure 2. Specimen and flaw geometry for rock-like material containing a single embedded flaw (2c=12.7mm).

3.3 Two and Three Flaws

Wong et al (2001) conducted laboratory experiments on simulated rock-like material containing two and three

embedded flaws (also of length 2c=12.7 mm) (Figure 3, Figure 4). The intact material had dimensions h:w:t of 120:60:25 mm with a UCS of 2.09 MPa, a tensile strength of 0.35 MPa, E of 330 MPa and Poisson's ratio of 0.19. The flaw bridge lengths for both the two and three flaw studies were held constant. In the case of the two flaw study, the flaw angle (α) and the bridge angle (β) were varied. In the three flaw study the flaw angle (α) and the second bridge angle (β_2) were varied, while the first bridge angle (β_2) was constant. Each of the orientations used flaws with a friction coefficient of 0.6 and was repeated using a flaw friction coefficient of 0.7.

Figure 3 shows the results for laboratory and PFC simulations for average crack initiation distance from flaw tip normalize to flaw half length. For flaw inclination angles between 30 and 45 degrees the numerical results were consistently lower, although possible results were limited due to geometrical restraints of the BPM noted above.

The study measured the peak strength of the two and three specimens with each flaw orientations and friction coefficient. The study also examined whether the crack coalescence was in shear, mixed (shear/tensile) or wing tensile mode.

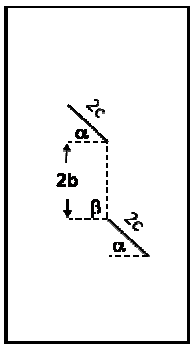

Test ID	α (°)	β (°)
2-1	45	45
2-2	45	75
2-3	45	90
2-4	45	105
2-5	45	120
2-6	65	45
2-7	65	75
2-8	65	90
2-9	65	105
2-10	65	120

Figure 3. Specimen geometry for a simulated rock-like material containing two embedded flaws of length 2c=12.7mm and bridge length 2b=20mm. Each geometry was tested with a flaws have a frictional coefficient of 0.6 and 0.7.

3.4 Strain Rate

The BPM is generally calibrated in a simulated uniaxial, biaxial, Brazilian or direct tension environment. One of the critical parameters selected in the testing environment is the platen strain rate. The ISRM suggested strain rate for triaxial testing is much lower than used in PFC due to the energy damping technique used. This technique ensures that the results of a PFC simulation in quasi-static conditions will be equivalent to those obtained in the lab using a much larger strain rate, enabling strain rates which are much higher than the laboratory. Even with this technique and with the current processor speeds of ~3.6 GHz for a reasonably sized BPM of 4000 particles may exceed simulation times of 24 hours, which may be unacceptable.

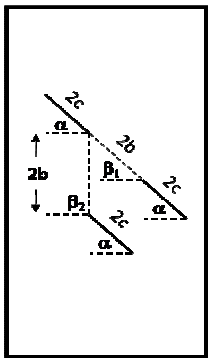

Test ID	α (°)	β_1 (°)	β_2 (°)
3-1	45	45	75
3-2	45	45	90
3-3	45	45	105
3-4	45	45	120
3-5	65	45	75
3-6	65	45	90
3-7	65	45	105
3-8	65	45	120

Figure 4. Specimen geometry for a simulated rock-like material containing three embedded flaws. Each geometry was tested with flaws having a frictional coefficient of 0.6 and 0.7.

Figure 5 shows the influence of strain rate on macroproperties values of the BPM. In each case the samples were not recalibrated. The SJ model crack initiation and coalescence may also be influenced by the strain rate, and thus the overall behaviour of the BPM with an SJ. Simulations on selected specimens were conducted in an attempt to improve simulation results and to investigate any behavioural discrepancies caused by strain rate variation.

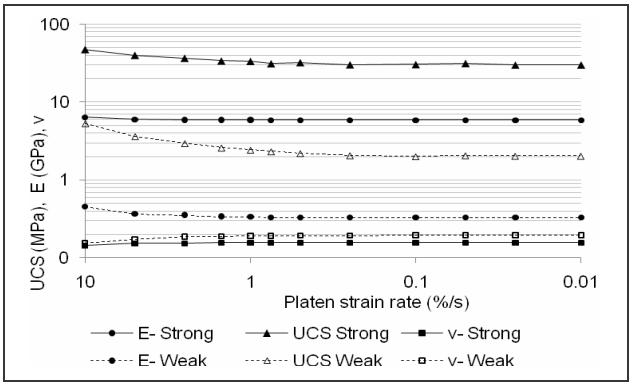

Figure 5. The influence of strain rate on compressive strength, Young's modulus and Poisson's ratio for weak and strong BPM samples under uniaxial compression.

4 RESULTS

All of the numerical tests were completed using the *Augmented Fish Tank (fist)* which was developed to create, test and extract the properties of a PFC2D BPM. On top of the *fist*, the *Virtual Laboratory Assistant* (*VLA*) was developed to easily create, test and extract the

properties of multiple combinations of PFC2D BPM materials, specimens, and testing parameters.

4.1 Material Calibration

The BPM must first be calibrated to match the intact macroproperties of the laboratory specimens through selection and testing of BPM microproperties. When calibrating the BPM for SRM applications, only the UCS, Young's (E) modulus and Poisson's ratio (v) are matched, therefore, it was decided to also only use these values for calibration of the above materials.

The strong (one flaw) and weak (two and three flaw) simulated rock-like material microproperties are listed in Table 1. The UCS and E were calculated using wall based measurements and v was calculated using measurements bases on gauge balls placed within the particle assembly. For each material the particle size ratio was 1.66 and the particle friction coefficient was 2.5. Only parallel bonds were used to create the BPM with the normal and shear parallel bond strength standard deviations set to 22.5% of the mean values. The remainder of the BPM microproperties were set to the default values. A friction coefficient of 0.36 was used for the platens with a testing strain rate of 0.25%/s. The resulting BPM macroproperties are listed in Table 2.

Table 1. Microproperties of the strong and weak materials (P – Particle, B – Bond).

Microproperties	Strong	Weak
Total Particles	6043	3747
Min. P Radius (μm)	564	564
P and B Modulus (MPa)	4020	235
P and B Stiffness Ratio	1.13	1.62
B Normal Strength (MPa)	30.9	1.71
B Shear Strength (MPa)	30.9	1.71

Table 2. Resulting BPM macroproperties of the strong and weak materials.

Macroproperties	Strong	Weak
E (GPa)	5970	328
v	0.151	0.191
UCS (MPa)	34.9	2.09
Direct Tension (MPa)	7.4	0.456

4.2 Smooth Joint Properties

The single flaw laboratory specimens were created through insertion of a thin metal sheet into the wet rock like material and removed creating an aperture of 0.1mm. The two and three flaw experiments used smooth and rough metal shims to create the flaws, while leaving them in during testing to create friction coefficients of 0.6 and 0.7 respectively.

The one flaw specimens were simulated with the SJ model friction coefficient set to zero with SJ normal and shear stiffness were set to 8.0 GPa/m. The two and three flaw specimens were simulated with SJ friction coefficients equal to those reported with SJ normal and shear stiffness of 10 GPa/m. For the samples with a friction coefficient of 0.7, a dilation angle of 4 was also used.

4.3 One Flaw Results

Figure 6 shows the results from the single flaw laboratory experiments with photographs and the corresponding SJ simulations. Only the simulation with the flaw orientated at α=75° did not reasonably match the observed laboratory behaviour. The remainder of the tests were not compared qualitatively as no photographs of the simulations were available. The mode of crack initiation and propagation (tensile wing crack, shear, or tensile) was not compared to the laboratory results.

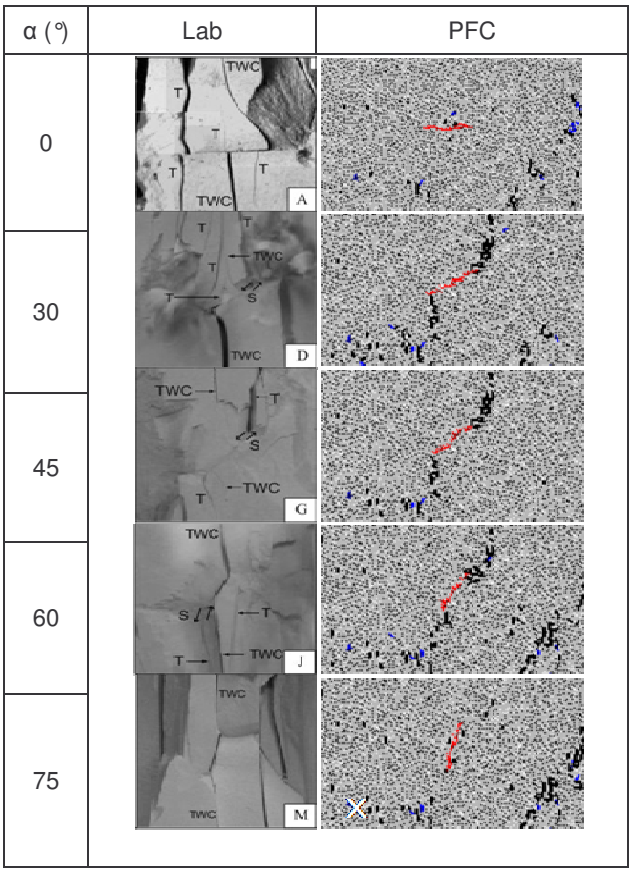

Figure 6. Results from SJ simulations on a single internal flaw compared with similar simulations conducted on laboratory specimens ('X' indicates no match). The red lines indicate the SJ model with tensile bond failure shown in black and shear failure shown in blue.

The laboratory experiments reported a series of measurements regarding the crack initiation distance from flaw tip and the angle of inclination of the crack relative to the flaw. Using only eight particles across the diameter of a flaw, crack initiation could only occur at four locations different locations on either side of the joint,

where *d* is measured from the flaw tip and $d \leq c$ (Figure 7). The angle of inclination of the crack is possible to measure, however it is a function of the BPM and not the crack initiation itself, and therefore not a good SJ performance indicator.

Figure 8 shows the results for laboratory and PFC simulations for average crack initiation distance from flaw tip normalized to *c*. For flaw inclination angles between 30 and 45 degrees the numerical results were consistently lower, although possible results were limited due to geometrical restraints of the BPM noted above.

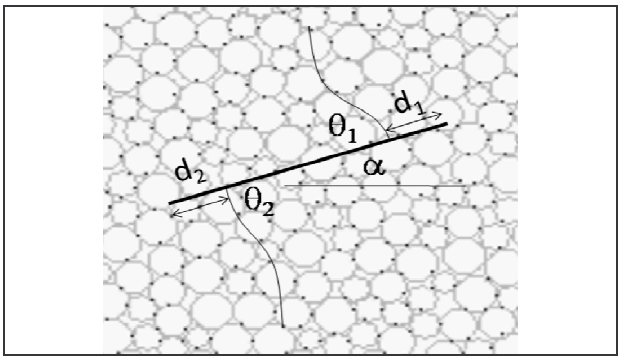

Figure 7. The measurement geometry for crack initiation from an internal flaw overlain on a BPM image. The crack initial distance (d_1 and d_2) are measured from the flaw tip.

4.4 Two and Three Flaw Results

Figure 9 shows the qualitative comparison between the observed laboratory behaviours of specimens containing two internal flaws with μ=0.6 and μ=0.7. The results from simulations 2-4 and 2-9 with μ=0.6 as well as 2-3 and 2-8 with μ=0.6 and μ=0.7 did not match the observed laboratory coalescence behaviours. The remainder of the simulations reasonably matched the observed behaviours.

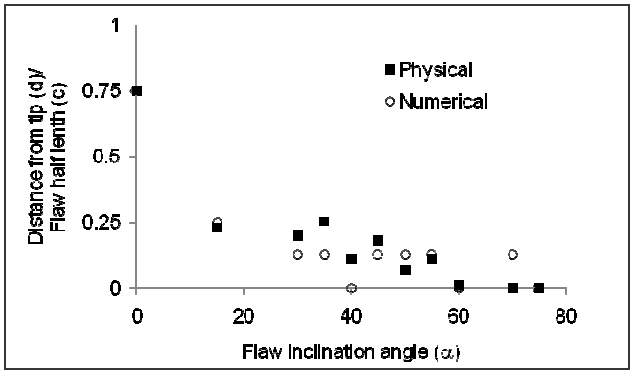

Figure 8. Measured crack initiation distances normalized to the flaw half length with the PFC results separated into shear or tensile bond failure at crack initiation.

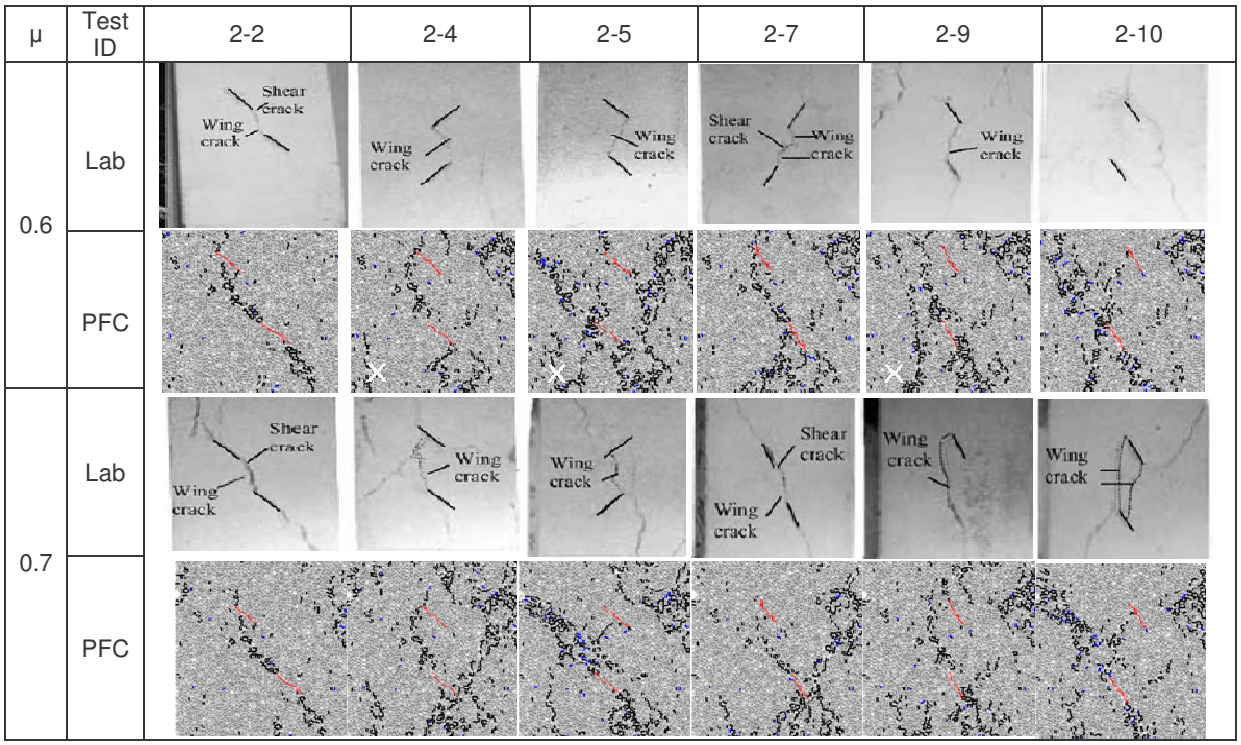

Figure 9. Laboratory and associated numerical simulation results on samples containing two internal flaws with friction coefficients of 0.6 and 0.7. Specimens with an 'X' did not match the observed laboratory results (SJ in Red and bond failure in black for tensile and blue for shear).

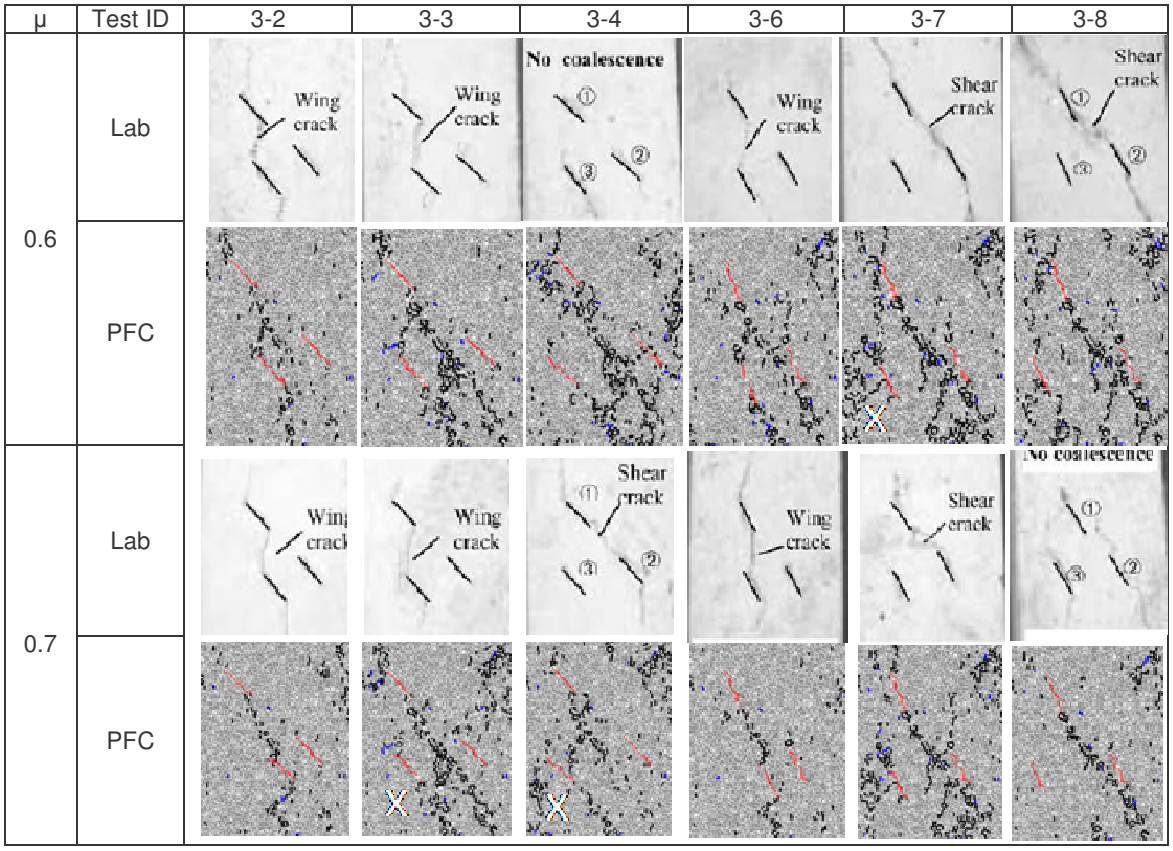

Figure 10. Laboratory and associated numerical simulation results on samples containing three internal flaws with friction coefficients of 0.6 and 0.7. Specimens with an 'X' did not match the observed laboratory results (SJ in Red and bond failure in black for tensile and blue for shear).

Figure 10 shows the qualitative results for laboratory and simulated three flaw specimens. Results for 3-3 and 3-4 with μ=0.7, 3-7 with μ=0.6 did not match the observed behaviour. The remainder of the simulations not shown did match the laboratory experiments. For specimen 3-3 it appears the wing crack from the bottom flaw will coalesce with the upper flaw however it does not even as the sample is taken well past peak strength.

The strength results were also recorded for each of the simulations and compared against the reported laboratory values (Table 3). In each case the strength results from the PFC SJ simulations were significantly higher than the corresponding laboratory values. The strength values did sometimes follow the increase and decrease in strength trends.

4.5 Strain Rate Results

Simulations on specimens 1-11, 2-4, 3-7 with μ=0.6, and 2-3, 3-3 μ=0.7 (which did not match the observed lab results) were re-run using a range of strain rates similar to Figure 5 to investigate if flaw coalescence would be altered or produce a better match to laboratory observations. The intact BPM was not recalibrated to the macroproperties of the laboratory specimen in both the strong and weak cases. The strain rates used were 5, 2.5, 1.5, 1, 0.75, 0.5, 0.1, 0.05 and 0.025 %/s.

Table 3. UCS results from laboratory and numerical simulations on specimens containing two and three internal flaws.

	Unconfined Compressive Strength (MPa)			
	μ=0.6		μ=0.7	
Test ID	Lab	PFC	Lab	PFC
2-1	1.67	2.00	1.88	2.07
2-2	1.59	1.91	1.80	1.99
2-3	1.59	1.81	1.57	1.87
2-4	1.88	2.06	1.84	2.07
2-5	1.64	1.99	1.73	2.04
2-6	1.42	1.96	1.44	1.96
2-7	1.45	2.01	1.49	2.00
2-8	1.49	1.97	1.48	1.97
2-9	1.51	2.05	1.52	2.06

2-10	1.46	2.00	1.48	2.00
3-1	1.59	1.90	1.73	2.03
3-2	1.57	1.97	1.73	2.04
3-3	1.60	1.93	1.61	2.03
3-4	1.69	1.97	1.70	2.03
3-5	1.43	2.01	1.58	1.93
3-6	1.42	1.93	1.52	2.07
3-7	1.51	2.01	1.62	2.00
3-8	1.51	2.00	1.58	2.02

Figure 11 shows the results from selected one, two and three flaw specimens. In each of the simulations the strain rate influenced the number of failed bonds and the mode of bond failure (shear or tensile). As the strain rate was reduced, the number of total bonds and the number of bonds failed in shear were reduced.

Single flaw test results with the varied strain rates did not provide improvements in matching the observed laboratory behaviours. The crack initiation and distance of crack initiation from the flaw tip was not accurately reproduced in the model for any of the applied strain rates. In the specimens containing two flaws that did not match the observed laboratory behaviour, the altering of the strain rate did not improve the results. The three flaw specimens also did not show any improved simulation performance with a reduced strain rate.

For the two and three flaw specimens, the flaw tips coalesced at a strain rate of 0.5 %/s, but did not coalesce for the remainder of the strain rates. In the remainder of the cases, the damage to the specimens bypassed the flaw before failure occurred.

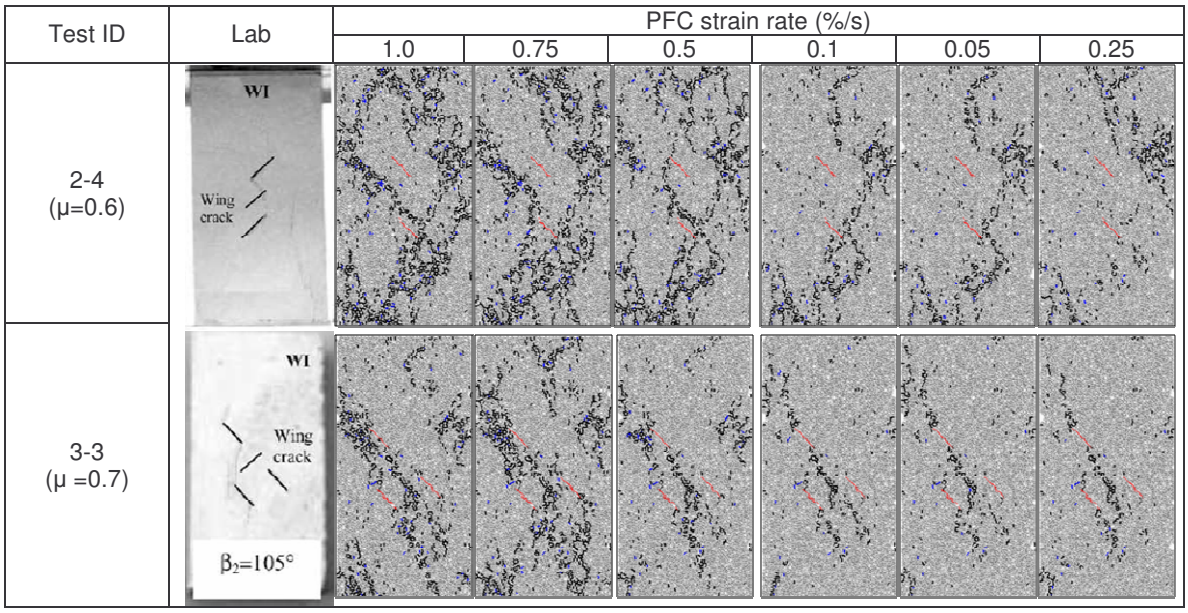

Figure 11. Results from BPM specimens containing two and three internal flaws and failed using varying strain rates

5 DISCUSSION

The numerical simulations on the behaviour of the SJ model versus observed laboratory behaviours produced acceptable results in general. The qualitative comparisons of crack initiation, propagation and coalescence versus observed laboratory behaviour provided an overall success rate of 73%. The strength results from the two and three flaw simulations overestimated the measured laboratory results. The strain rate was shown to have an impact on failure of the samples, but only slightly altered the behaviour of the sample with regards to the SJ model.

5.1 Crack Initiation, Propagation, and Coalescence

For the one flaw, two flaw and three flaw numerical specimens, the crack initiation, propagation and coalescence was simulated reasonably well. The single flaw laboratory results were able to be reproduced with an 80% success rate. The two and three flaw results were able to be reproduced with 65% and 81% success rate respectively.

The crack initiation distances measured from the flaw tip for the single flaw specimens also produced acceptable results. As the average measured crack initiation distance was below 0.25 in many of the cases, the results were constrained by the geometry of the simulated flaw. Therefore, if the crack initiated from the flaw at either the flaw tip, or one particle away from the flaw tip, the results can be considered successful. In all but one case, the observed laboratory results did not match the crack initiation and failure.

The two and three flaw specimens matched the observed flaw behaviour well. In some of the simulated specimens (2-4, 2-5, 3-4, 3-7) the simulated behaviour did not match the laboratory behaviour, however the internal flaws did coalesce and influence the failure

behaviour of the specimen. The cases which did not match adequately may be improved by altering the particle arrangements. Each simulation used the same initial sample to insert the SJ model. Varying the packing between samples randomly may produce different behaviours.

5.2 Strength

The strength results of the two and three flaw simulations are consistently higher than those reported from the laboratory simulations. The crack initiation and propagation is a tensile failure process and the BPM is known not to properly reproduce UCS to tensile strength ratios when using circular (2D) or spherical (3D) particle shapes. The BPM was calibrated without considering the tensile strength, and then measuring the tensile strength upon calibration completion, resulting in a tensile strength 1.30 times greater than the laboratory specimens. The average strength of the simulated specimens was found to be 1.26 times greater than the measured laboratory specimens, with no changes from the two to three flaw strength averages.

Crack initiation from a pre-existing internal flaw is predominantly tensile failure and PFC does not simulate tensile to UCS strength ratios well (Wong et al., 2001). Recent work has demonstrated that the changing the shapes of the particles, were instead of using spherical shapes, multiple shapes may be bonded together to provide non-spherical shapes, called “clumps” (Cho, N., 2008). Tests on PFC clumped materials have shown to better represent the tensile to UCS strength ratios shown in the laboratory. Clump material types are currently not capable of supporting the SJ model. Therefore, incorporating the SJ model into a clumped material with a better tensile-UCS strength ratio, or if an improvement on the tensile-UCS strength ratio for the spherical BPM can be made, better results for the strength and perhaps the flaw behaviour may be seen.

5.3 Influence of Strain Rate

The strain rate of the numerical UCS test was shown to have an influence on the behaviour of the BPM with and without the SJ model. The reduction in strain rate on the BPM caused a decrease in the observed strength. This behaviour can be explained as an artefact of the dynamic nature of the PFC calculation method.

6 CONCLUSIONS

The SJ model has been shown to reasonably reproduce observed laboratory internal flaw behaviours, crack initiation, propagation and coalescence behaviours. This provides an increase in confidence that the SJ is behaving acceptably inside of the SRM. There is concern that the strength values reproduced in the experiments do not match laboratory behaviours, and that calibrating the BPM only to the UCS, E and v may not be sufficient to capture observed material behaviours. Simulations using the SJ model within a BPM made up of non-spherical clumped shapes may also improve the overall behaviour and the SJ model should be adapted to work with these materials.

7 ACKNOWLEDGEMENTS

The writers would like to acknowledge the contributions and ageless enthusiasm of Professor Charles Fairhurst.

REFERENCES

Cho, N. 2008. Ph D Thesis. Discrete Element Modeling of rock: pre-peak fracturing and dilation. *U. of Alberta.*

Fairhurst C., Damjanac B., and Brandshaeg T., 2007. “Rock Mass Strength and Numerical Experiments**.”** 35th Geomechanics Colloquium. Tech. Univ. Freiberg, Institutsheft Geotechnik 2006 – 5.

Itasca Consulting Group Inc. 2008. PFC2D - Particle Flow Code in 2 Dimensions, Version 4.0 Minneapolis, ICG.

Mas Ivars D., Deisman N., Pierce M., and Fairhurst C. 2007. The synthetic rock mass approach – a step forward in the characterization of jointed rock masses. *in The Second Half Century of Rock Mechanics (11th Congress of the International Society for Rock Mechanics, Lisbon, July 2007)*.

Pierce M., Cundall P., Darcel, C., Min, K., Potyondy, D., Young, R.P., Reyes-Montes, J. & Pettitt, W. 2005. Six Monthly Technical Report, Caving Mechanics, Sub-Project No. 4.2: Research and Methodology Improvement, & Sub-Project 4.3, Case Study Application. *ICG Report to Mass Mining Technology Project, 2004-2007, September*.

Pierce M., Cundall P., Potyondy D., and Mas Ivars D. 2007. A synthetic rock mass model for jointed rock. *in Rock Mechanics: Meeting Society's Challenges and Demands (1st Canada-U.S. Rock Mechanics Symposium, Vancouver, May 2007)*.

Potyondy, D. and Cundall, P. 2004. A bonded-particle model for rock. *Int. J. Rock Mech. Min. Sci*., 41, 1329-1364.

Wong, L.N.Y. and Einstein, H.H. 2006. Fracturing behaviour of prismatic specimens containing single flaws. *In ARMA/USRMS 06-899*.

Wong, R.H.C., Chau K.T., Tang C.A., and Lin P. 2001. Analysis of crack coalescence in rock-like materials containing three flaws – Part 1: Experimental approach. *Int. J. Rock Mech. Min. Sci*., 38, 909-924.